THE JOURNAL OF PHYSICAL CHEMISTRY C

Article

Cite This: J. Phys. Chem. C 2019, 123, 13410−13418

pubs.acs.org/JPCC

Stationary and Dynamical Properties of Polarons in Anisotropic C_{60}-Crystals

Marcelo Lopes Pereira, Jr.,[†] Wiliam Ferreira da Cunha,[†] Rafael Timóteo de Sousa, Jr.,[‡] Geraldo Magela e Silva,[†] and Luiz Antonio Ribeiro, Jr.*[,†]

[†]Institute of Physics, University of Brasília, Brasília 70910-900, Brasília, Brazil

[‡]Department of Electrical Engineering, University of Brasília, CP04455, Brasília 70919-970, Brazil

Supporting Information

ABSTRACT: Two-dimensional C_{60} crystals are treated with a Holstein−Peierls model that takes into account both intra- and intermolecular vibrational modes to describe charge transport. By virtue of this procedure, we obtained the set of values for intra- and intermolecular electron−phonon coupling that makes it possible to study stationary properties of polarons as well as to investigate the transport regime of the charge carriers. This is carried out by considering the presence of anisotropy of electronic terms and effects because of the application of external electric fields. We have mapped the regimes in which polarons of different nature—each endowing the system with different properties—are observed.

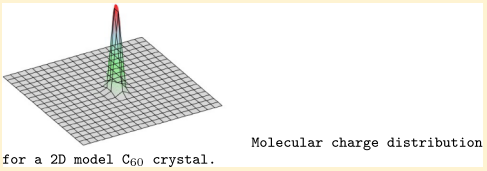

INTRODUCTION

Organic semiconductors have received great attention from industry and the scientific community since the discovery of conducting polymers in the second half of the 20th century.[1,2] These materials are exciting potential replacements for inorganic materials as far as the manufacture of devices that capture, control, and emit light[3] is concerned. Indeed, organic optoelectronics has a significant number of advantages over inorganic devices: favorable mechanical properties, with the possibility of making thinner and more malleable devices; superior optical properties, enabling the production of transparent devices; and a more sustainable energy generation and fabrication process, which is dependent on abundant resources and includes the possibility of recycling,[4−9] are just a few of the many points that deserve mentioning.

Organic semiconductors can be broadly divided into three major categories: organic polymers, amorphous films, and molecular crystals. Among these classes, charge carriers in the latter are the ones that tend to present the highest mobility and have, for this reason, been the go to material to conceive the next generation of high-performance organic field-effect transistors.[10] Molecular crystals are quasi-crystalline materials whose unit cells are composed of whole molecules, instead of one or two isolated atomic species. These molecules interact via several different interactions, the most common not only being of van der Waals (vdW) nature but also being possible to be mediated through multipole interactions, π-stacking, hydrogen bonds, London dispersion forces, and others. Some of the interesting properties of organic molecular crystals comes from the fact that although inside the unit cell, strong covalent interactions make the system stable, the weak interaction—such as vdW—between cells provides flexibility to the material. From this consideration follows the fact that organic molecular crystals make up a class of organic semiconductors that present two main types of vibrational modes: intramolecular modes (Holstein type) originated from the strong C−C bonds and usually considered in an harmonic approximation (provided the displacements are not too large) and intermolecular modes (Peierls type) governed by vdW interactions and typically modeled by Lennard-Jones potentials.[11,12] This class of system has been extensively studied in the scope of charge transport[13−20] because of the interest of the scientific community on these systems and the importance of their properties. The idea is that a deep understanding of the transport mechanism is a necessary condition to achieve higher efficiency of organic optoelectronic devices.

Among the constituents that can form crystals of interesting properties, a specific molecule is specially promising: C_{60}, also known as buckminsterfullerene. Isolated C_{60} molecules are stable species that present a high electron affinity and a number of favorable mechanical properties. This makes them good candidates to electron acceptors in bulk heterojunction photovoltaics,[21] among other uses.[22,23] Because of the high range of potential applications, this system has been, by itself, the focus of many discussions from the scientific community. Although the very possibility of the stability of molecular crystal based in C_{60} dates from over a decade,[24] it was not until recently that the stability of such compound has been definitively established,[25] thus opening the path for a whole new avenue of possibilities in the field of organic electronics. Necessary to the development of this technology is a comprehensive understanding regarding the charge transport in the material.

Received: January 23, 2019
Revised: May 14, 2019
Published: May 17, 2019

DOI: 10.1021/acs.jpcc.9b00705
J. Phys. Chem. C 2019, 123, 13410−13418

Some interesting works regarding charge transference have dealt with C_{60} clusters, rather than the crystal. For instance, Tamura and Tsukada had studied the electron transport in C_{60} aggregates using density functional theory to obtain electronic transfer integral and vibration coupling, with calculations of quantum dynamics based on a parametrization from first principles. They presented the electronic transfer integral for the three possible cases of interaction between molecules of C_{60}, that is, when the polygon parallel to two molecules of C_{60} contained two, five, or six carbon atoms. It was shown that the electronic transfer integral is an anisotropic term, with one direction corresponding to approximately 10% of the value in another direction.[26] Undoubtedly, their effort consists in a first step toward the understanding of charge transport in a C_{60}, although falling considerably short from the molecular solid picture. Indeed, the crystal orientation and the interaction of several sites are expected to provide the system with drastically different properties, such as possible quasi-particle description. Still, there is a lot of merit in their work, particularly when showing the importance of considering anisotropy and on pointing for the need to investigate the charge transport behavior. The most immediate gap to be filled consists of studying the transport picture in actual C_{60} solids, considering anisotropy and the effect of the interaction between the electronic and the lattice degrees of freedom of the system.

In this work, we tackle this issue by considering a Holstein–Peierls type model that is applied to a two-dimensional C_{60} crystal in order to investigate charge transport within the system in the framework of a Ehrenfest molecular dynamics. Importantly, Zhao and co-workers have developed a numerical exact method—named Dirac–Frenkel time-dependent variational approach with the Davydov Ansatz—where the accuracy of the simulated dynamics is significantly enhanced in comparison with the semi-classical Ehrenfest dynamics.[27−39] Nevertheless, the results obtained in our previous studies[17−19] ensure that the method developed by us can predict, qualitatively, the stationary and dynamical properties of polarons in model organic crystals. In this sense, we begin by studying the influence of electron–phonon (e–ph) coupling on the static properties of the system and, through this approach, observed that, depending on the system's parameters, a quasi-particle mechanism is observed. In other words, we describe the combination of parameters that make it possible for polarons to arise as charge carriers. After this static characterization, we performed an analysis on the system's dynamics. By applying external electric fields together with the presence of anisotropy on both directions of the crystal, the response of the charge carrier is investigated. We found that, depending on the very combination of these parameters, polarons of different natures are obtained, thus providing the system with different properties.

METHODOLOGY

In our calculations, the C_{60} crystal is approximated by a two-dimensional molecular matrix in which each site of the system represents a C_{60} molecule in its i (line) and j (column) address, as described by Figure 1. The monolayer intermolecular interacting nature of the model considers each site interacting with four neighbors. Our representation considers two types of electron–lattice interactions. The local intramolecular mode with displacement $u_{i,j}$ is coupled to the electronic system by the intramolecular e–ph coupling α_1, whereas the intermolecular interactions are inserted by means

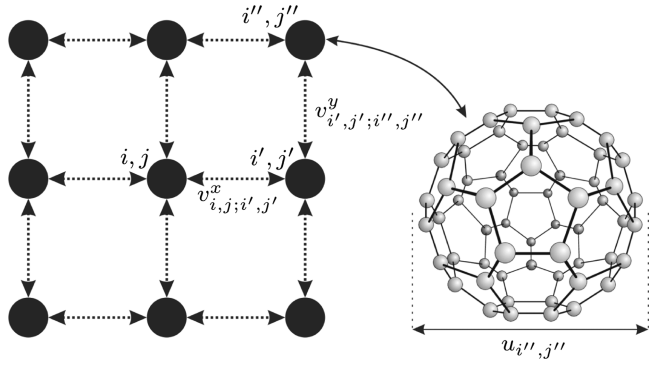

Figure 1. Representation of the Holstein–Peierls model of the system: a two-dimensional molecular matrix. Here, $v^{x}_{i,j;i'j'}$ and $v^{y}_{i,j;i'j'}$ represent the displacement of the (i,j) site regarding the next-neighboring (i',j') site in the directions x and y, respectively, whereas $u_{i,j}$ shows the distortion of the site (i,j).

of transfer integrals $J^{x,y}_{i,j;i',j'}$ between neighboring sites (i,j) and (i',j'), with displacements $v^{x}_{i,j}$ and $v^{y}_{i,j}$. Such variables are obtained from the displacement of a molecule, from equilibrium, relative to the adjacent, which are coupled by the intermolecular e–ph coupling $\alpha^{x,y}_2$, in the x and y directions, respectively, as shown in Figure 1.

From the representation discussed above, the total Hamiltonian of the system is given by

$$H = H_{\text{elec}} + H_{\text{latt}} = H_{\text{elec,intra}} + H_{\text{elec,inter}} + H_{\text{latt,intra}} + H_{\text{latt,inter}} \quad (1)$$

with

$$H_{\text{elec,intra}} = \sum_{i,j} \alpha_1 u_{i,j} \hat{c}^{\dagger}_{i,j} \hat{c}_{i,j} \quad (2)$$

and

$$H_{\text{elec,inter}} = \sum_{i,j} (J^{x}_{i,j+1;i,j} \hat{c}^{\dagger}_{i,j} \hat{c}_{i,j+1} + \text{H. C.}) + \sum_{i,j} (J^{y}_{i+1,j;i,j} \hat{c}^{\dagger}_{i,j} \hat{c}_{i+1,j} + \text{H. C.}) \quad (3)$$

The operators $\hat{c}^{\dagger}_{i,j}$ ($\hat{c}_{i,j}$) create (annihilates) an electron on the (i,j) site of the molecular matrix. The lattice treatment based on two separate harmonic oscillators is given by

$$H_{\text{latt,intra}} = \frac{1}{2} K_1 \sum_{i,j} (u_{i,j})^2 + \frac{1}{2} M_1 \sum_{i,j} (\dot{u}_{i,j})^2 \quad (4)$$

and

$$H_{\text{latt,inter}} = \frac{1}{2} K_2 \sum_{i,j} (v^{x}_{i,j+1} - v^{x}_{i,j})^2 + \frac{1}{2} K_2 \sum_{i,j} (v^{y}_{i+1,j} - v^{y}_{i,j})^2 + \frac{1}{2} M_2 \sum_{i,j} [(\dot{v}^{x}_{i,j})^2 + (\dot{v}^{y}_{i,j})^2] \quad (5)$$

where force constants K_1 and K_2 and masses M_1 and M_2 refer to the intra- and intermolecular oscillators, respectively.

The electric field is assumed to be static and is implemented in the x-direction, being included in the model by a time-dependent vector potential $A_x(t) = -cE_{0x}t$ so that electronic transfer integrals are defined by

$$J^{x}_{i,j+1;i,j} = (J^{x}_{0} - \alpha^{x}_{2}(v^{x}_{i,j+1} - v^{x}_{i,j})) \exp(i\gamma A_x(t)) \quad (6)$$

DOI: 10.1021/acs.jpcc.9b00705
J. Phys. Chem. C 2019, 123, 13410−13418

and

$$J^{y}_{i+1,j;i,j} = J^{y}_{0} - \alpha_2^{y}(v^{y}_{i+1,j} - v^{y}_{i,j}) \tag{7}$$

E_{0x} is the electric field strength, and $\gamma = ea/\hbar c$, where e is the absolute electronic charge, a is the lattice constant, and c is the speed of light.

In this work, the focus is the analysis of the values of the intra- and intermolecular e−ph couplings and their influence on polarons of isotropic and anisotropic systems. The polaron dynamics is also investigated considering the anisotropy of the system under different external electric field regimes. Here, the following set of parameters are adopted: $J^{x}_{0} = 100$ meV, J^{y}_{0} varies in the interval [0−100] meV, α_1 and α_2 vary in the interval [0−5] eV Å^{-1}, $K_1 = 16.51$ eV Å^{-2}, $K_2 = 0.51$ eV Å^{-2}, $M_1 = 7.5 \times 10^{10}$ eV(as/Å)^2, $M_2 = 1.5 \times 10^{11}$ eV(as/Å)^2, $a = 3.0$ Å, and E_{0x} varies in the interval [0.8−3.2] mV/Å. All simulations were performed in 20 × 20 lattices with periodic boundary conditions. The parameters used here were obtained from our calculations and also from other successful theoretical and experimental works.[26,40−46] Importantly, the geometry of the system is optimized using the resilient backpropagation, RPROP, algorithm.[47] The equations and the procedure adopted here to obtain the initial geometry are well described in ref 12.

The electronic dynamics is described by the time-dependent Schrödinger equation (TDSE)

$$i\hbar\dot{\psi}(i, j, t) = H_{\text{elec}}\psi(i, j, t) \tag{8}$$

By introducing instantaneous eigenstates, the solution of TDSE at each instant can be expressed in the form

$$\psi(i, j, t + \Delta t) = \sum_{l}\left[\sum_{i',j'}\phi_l^{*}(i', j')\psi(i', j', t)\right] \times e^{\delta}\phi_l(i, j) \tag{9}$$

with $\delta = -i\varepsilon_l\Delta t/\hbar$. $\phi_l(i,j)$ and ε_l are the instantaneous eigenfunctions and eigenvalues for the electronic part of the Hamiltonian at a given time t, respectively.[48]

Newtonian equations of motion for the molecules in the molecular array govern the intramolecular displacements with

$$F_u \equiv M_1\ddot{u}_{i,j}(t) = -K_1u_{i,j}(t) - \frac{\alpha_1}{M_1}\rho_{i,j;i,j}(t) \tag{10}$$

and the intermolecular displacements

$$M_2\ddot{v}^{x}_{i,j}(t) = F_{v^x}$$

$$= -K_2(2v^{x}_{i,j}(t) - v^{x}_{i,j+1}(t) - v^{x}_{i,j-1(t)}) - \frac{\alpha_2^{x}}{M_2}e^{-i\gamma A_x(t)}(\rho_{i,j;i,j-1}(t) - \rho_{i,j+1;i,j}(t)) - \frac{\alpha_2^{x}}{M_2}e^{i\gamma A_x(t)}(\rho_{i,j-1;i,j}(t) - \rho_{i,j;i,j+1}(t)) \tag{11}$$

and

$$M_2\ddot{v}^{y}_{i,j}(t) = F_{v^y}$$

$$= -K_2(2v^{y}_{i,j}(t) - v^{y}_{i+1,j}(t) - v^{y}_{i-1,j(t)}) - \frac{\alpha_2^{y}}{M_2}(\rho_{i,j;i-1,j}(t) - \rho_{i+1,j;i,j}(t)) - \frac{\alpha_2^{y}}{M_2}(\rho_{i-1,j;i,j}(t) - \rho_{i,j;i+1,j}(t)) \tag{12}$$

where $\rho_{i,j;i',j'}(t)$ is the electron density matrix given by

$$\rho_{i,j;i',j'}(t) = \psi_{i,j}(t)\psi^{*}_{i',j'}(t) \tag{13}$$

It is well known that the C_{60} molecules are found to be arranged in a perfect hexagonal pattern within a crystalline structure.[49] However, in our model for the C_{60} crystal, each molecule has only two neighbors in x- and y-directions following the orientation of the applied electric field. In the context of this approach, the charge localized in a particular molecule can drift only to its next-neighboring one according to the direction of the electric field. Moreover, most of the charge lies in a unit of the molecular crystal, and the next-neighboring ones (in both directions) share the small remaining part. Consequently, the polaron transport occurs in the linear direction where most of the molecular charge is placed. The square lattice is convenient approximation for the number of neighbors and the fixed direction for the applied electric field. In this kind of approach, only two neighbors are neglected regarding the hexagonal lattice. These neighbors are always out of the polaron transporting line because of the orientation of the applied electric field. We believe that, if a square lattice were stable, there would be a small difference in the polaron localization regarding the hexagonal lattice. In organic materials, different charge localizations lead to variances in the carrier's effective mass that, consequently, would change its drift velocity. Quantitatively, there would be a small difference between the two lattices when it comes to the polaron localization and its underlying properties. However, the charge transport mechanism would be qualitatively the same.

RESULTS

In this section, we present the findings and discussions regarding the charge transport in C_{60}-crystals. All of the calculations were performed in a 20 × 20 molecular crystal with periodic boundary conditions. We should point out that we have also performed preliminary calculations for other sizes of the molecular crystal. The results presented here, however, provided the best compromise between accuracy of the data and computational feasibility.

The constraint of periodic boundary conditions is enforced by

$$\sum_{j} v^{x}_{i,j+1} - v^{x}_{i,j} = \sum_{i} v^{y}_{i+1,j} - v^{y}_{i,j} = 0 \tag{14}$$

In order to allow for a better understanding of our results, we divide the present section into two subsections: the first one considers the influence of intra- and inter-e−ph coupling on polaron stability as well as on the kind of charge carrier generated and the second exploits the effects of external electric field and anisotropy on polaron dynamics.

DOI: 10.1021/acs.jpcc.9b00705
J. Phys. Chem. C 2019, 123, 13410−13418

Polaron Nature and Stability. By considering the Holstein−Peierls model, we are taking the intra- and intersite contributions into account. For a quasi-particle solution to arise in analogy with what happens in other organic semiconductors,[50,51] the degrees of freedom of the electronic part must be coupled to those of the lattice. In our model, this is accomplished by the presence of the e−ph coupling constant, whose value, although not yet reported in the literature for the given system, is crucial to the understanding of the charge transport mechanism in organic crystals. It is to say: depending on such values, a more localized or more delocalized charge distribution can be obtained. In order to assess to what degree a given localization corresponds to a quasi-particle, as well as to determine the kind of the obtained structure, we consider the inverse participation radius (IPR) defined as

$$\mathrm{IPR} = \frac{\sum_{i,j} |\rho_{i,j}|^2}{\left(\sum_{i,j} |\rho_{i,j}|\right)^2} \tag{15}$$

The IPR is a dimensionless charge localization measure in the sense that the more spread the charge in the lattice, the lower the IPR. It varies from 0.0, indicating a completely delocalized charge, to 1.0 associated with complete localization. This is clearly a function of both the intra- and intermolecular e−ph couplings, as shown in Figure 2, which

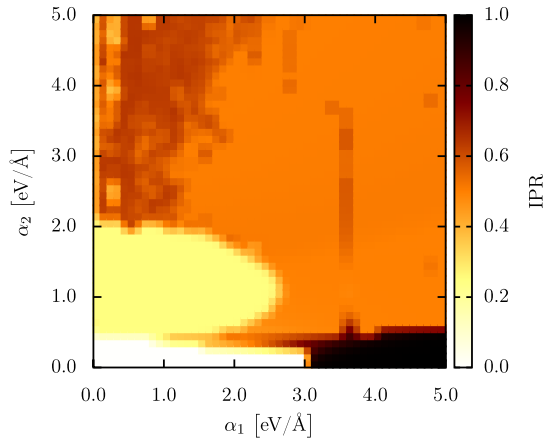

Figure 2. IPR as a function of α_1 and α_2. Four different regimes, associated with polarons of different natures, are observed depending on the combination of e−ph couplings.

represents a mapping between these parameters and the IPR. As can be noted, the system's IPR depends on both the charge distribution and the geometry characteristic of each state.

The analysis of IPR conducted from Figure 2 shows that there are four distinct types of polaron solution in these systems depending on the combination of the e−ph constants employed. The first regime (represented by the white region) consists of small values of α_1 (<3.0 eV Å^{-1} and α_2 (<0.5 eV Å^{-1}) that do not present enough magnitude to trap the amount of extra charge that originates the polaron. For this reason, it is called a free-electron-like solution, that is, there is no formation of polarons. A distinct pattern arises for the region associated with small α_1 (<2.5 eV Å^{-1}) but intermediate values of α_2 (between 0.5 and 2 eV Å^{-1}). In this case, a metastable polaron solution is achieved because of the intermolecular entrapment of charge caused by the respective lattice deformation. Because of the small intramolecular coupling, however, the physical solution is not dynamically stable in the presence of an external electric field. Moreover, even in the stationary case, in the presence of anisotropy, this solution is not obtained, where in the isotropic case, the electronic charge density is distributed in four sites. The region with α_1 large (>3 eV Å^{-1}) and small α_2 (<0.5 eV Å^{-1}) has a "small polaron" solution (or Holstein polaron solution[52,53]), in which the IPR is higher than 0.75, and the additional charge of the system is mainly concentrated in a single molecular unit. This is due to the fact that α_1 large and α_2 small reflect the charge being strongly coupled to the intramolecular distortions of the system but feeling intermolecular deformations of the lattice very little. This results on the imprisonment of charge into a single molecular unit. Finally, the orange colored region is known as the "large polaron" solution (or Fröhlich polaron solution[54]). It corresponds to an IPR between 0.4 and 0.75, with the excess charge on the crystal mainly distributed in a central molecular unit and the remainder in its first four neighbors. This solution locally polarizes the system, involving approximately five lattice sites. This solution proves to be the most dynamically stable among the four types of solution. As a remark, one can clearly see that depending on the relation between the two e−ph constants, rather different charge distributions are obtained which, in turn, is reflected in systems with different transport properties.

From the previous results on the localization of charge as a function of the e−ph couplings, we adopt the values of α_1 = 3.0 eV Å^{-1} and α_2 = 0.4 eV Å^{-1} to specifically describe the properties of a characteristic large polaron solution in organic crystals of C_{60}. In Figure 3, we further characterize the system

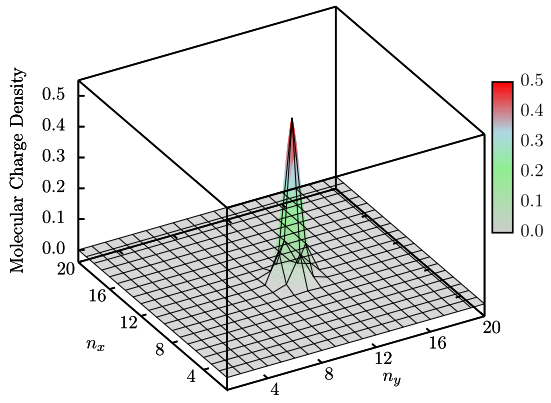

Figure 3. Molecular charge density in an isotropic C_{60} molecular crystal with α_1 = 3.0 eV Å^{-1} and α_2 = 0.4 eV Å^{-1}.

now in terms of symmetry arguments over the charge displacement. It can be seen that 0.5 e is located in a single central unit, whereas approximately 0.4 e is equally distributed among its nearest four neighbors. The intramolecular distortions and intermolecular deformations observed here are qualitatively similar to the ones previously presented in the literature.

As it would be expected, the geometry of the system changes when anisotropy is taken into account. We carried out several simulations by varying J_0^y in the interval [0−100] meV and look at the IPR to understand the polaron localization in the system for different degrees of anisotropy. Table 1 presents the values obtained and from that one can conclude that there are only two types of polaron configuration in the entire observed

DOI: 10.1021/acs.jpcc.9b00705
J. Phys. Chem. C 2019, 123, 13410−13418

Table 1. IPR as a Function of J_0^y

J_0^y [meV]	IPR
0	0.49744
10	0.49743
20	0.49734
30	0.49706
40	0.49634
50	0.49485
60	0.49215
65	**0.49020**
66	**0.79653**
70	0.79630
80	0.79040
90	0.77716
100	0.75799

anisotropy spam: from 66 meV (intermediate anisotropy) to 100 meV (no anisotropy), the IPR lies in the range of 0.75−0.79. This corresponds to a large polaron solution with two-dimensional characteristics, as shown in Figure 3. It has a slight change in the molecular charge density in the two molecules near the polaron center through the *y*-direction. The charge density in these two molecular units decreases slightly, with the charge being transferred to the central unit of polaron. On the other hand, for J_0^y ranging from 0 (high anisotropy) to 65 meV (intermediate anisotropy), although the solution remains that of the large polaron type, it presents one-dimensional characteristics, and the center of the polaron now consists of two molecular units, containing approximately 0.35 e each. The remaining 0.3 e is equally distributed among the six neighbors of the two polaron core molecules (0.05 e each), as can be observed in the upper left panel of Figure 4. It presents the deformations of the crystalline lattice in the presence of additional charge. The upper right panel presents the intramolecular distortions of the system, from which a behavior very similar—only opposite in sign—to that of the molecular charge density can be inferred. The negative values indicate that the molecules compress proportionally to the presence of charge density. The lower left panel shows the bonding length of the molecules in the *x* direction ($v_{i,j+1}^x - v_{i,j}^x$). The presence of the additional charge can be attributed to the two molecules that compose the polaron, and as a result, the other sites of the same molecular line have moved away because of the approximation of the molecules to the polaron center. The lower right panel represents the bond lengths in *y* direction ($v_{i+1,j}^y - v_{i,j}^y$), which have lower intensity due to the implemented anisotropy of the system. Because the probability amplitude of the hopping of the electron is smaller in one direction, the deformations of the system in that direction will correspondingly decrease. Note that in the *y* direction, two molecular columns undergo deformations, distancing themselves from one another when far from the center of the polaron. This is due to the approximation of the molecules near the molecular charge center. It is also worthy to mention that once the deformation intensity is lower, the effective mass of the polaron is even smaller, making anisotropic systems more propitious to transport, as will be discussed later.

It is worthwhile to highlight that Figures 3 and 4 present essential aspects related to the charge localization and lattice configuration for our model lattice containing a polaron. As depicted in Figure 3, the polaronic charge lies in five molecules with its main contribution (approximately 48%) residing on a single central site. When it comes to the intermolecular relative displacements, it is possible to note in Figure 4 that there is a contraction (negative displacements) presented by the two next-neighboring molecules regarding the central one containing the polaronic charge. These contractions are followed by expansions (positive displacements) on the direction through the row of the molecular array where the central molecule is localized. We have noted that the dynamical properties for the polaron do not change when we consider bigger lattices no matter what the reach of the bond elongations within the row of the molecular array containing the central polaron molecule.

Polaron Dynamics. We are now in the position of describing the time-dependent behavior of the quasi-particles in C_{60} crystals. Polarons of different nature, such as discussed in the previous section, are expected to possess different properties as far as their dynamics is concerned. Therefore, after obtaining a given static solution depending on the parameters chosen, we evolved the system in time using the Ehrenfest molecular dynamics methodology. This is accomplished in the presence of external electric field and electronic anisotropy, both for the transfer integral and for the

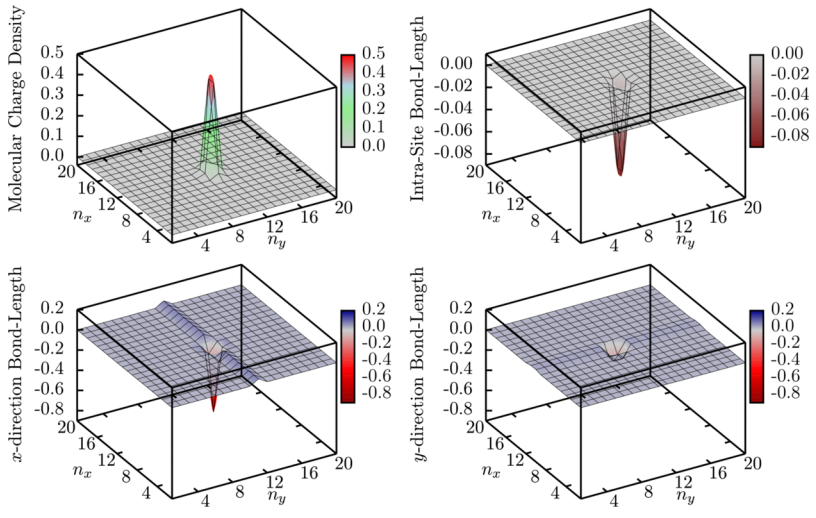

Figure 4. Polaron geometry in anisotropic two-dimensional C_{60} system with J_0^y = 50 meV, α_1 = 3.0 eV Å^{-1} and α_2 = 0.4 eV Å^{-1}.

DOI: 10.1021/acs.jpcc.9b00705
J. Phys. Chem. C 2019, 123, 13410−13418

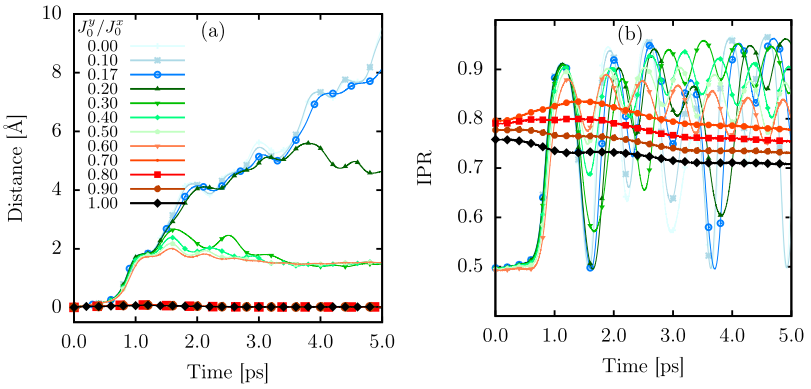

Figure 5. Time evolution of (a) molecular charge center and (b) IPR, for different anisotropy regimes, with external electric field of intensity of 2.0 mV/Å.

intermolecular e−ph coupling. In order to do so, we use the set of parameters presented in the Methodology with standard values of α_1 = 3.0 eV Å^{-1} and α_2 = 0.4 eV Å^{-1}. The dynamics evolution of the system is obtained from Euler−Lagrange equations, which are integrated using the Brünger−Brooks−Karplus integrator.[55,56]

In this work, we chose to investigate the time evolution of the charge carrier by defining its molecular charge center. This is done by resorting to the following average

$$x_p(t) = \frac{Na}{2\pi} \arg\left(\sum_{l=1}^{N} \exp\left(\frac{2\pi i l}{N}\right)\overline{\rho}_l(t)\right) \tag{16}$$

where N is the number of molecules and a is the lattice constant. ρ_l is the one-dimensional charge density. By tracking this quantity, we follow a representative description of the polaron while it moves through the lattice. Please note that the polaron velocity is derived from the position of its center of mass (x_p).

For a fixed external electric field of 2.0 mV/Å, Figure 5 presents the time evolution of the molecular charge center for different degrees of anisotropy in the main panel (panel a) as well as the evolution of the IPR for each case in the inset (panel b). Each line corresponds to a given ratio of J_0^y as compared to J_0^x. When these two quantities are equal, it means that the lattice is isotropic. A clear aspect to be noted from this figure is the presence of well-defined phase transitions in the transport behavior of the polaron depending on the anisotropy pattern. Note that for high degrees of isotropy, the polaron cannot hop, so that there is no transport. This occurs for $J_0^y >$ 65 meV, which agrees with Table 1, showing that for polaron solutions qualitatively similar to that presented in Figure 3, there is no polaron dynamics. This is due to the high value of the effective mass of the charge carrier, which cannot displace all deformations in the y-direction along with the additional charge (which is coupled to the distortions due to e−ph coupling). This result is reinforced by the data in panel b, where it can be observed that for higher transfer integrals in y-direction (lower anisotropy and higher values of IPR due to the fact that the polaron is wider when it is mainly in a single direction), the IPR varies little in time, showing only the relaxation−compression of the polaron because of the energy gain of the electric field, but without being able to perform a leap from one molecule to another. On the other hand, for J_0^y between 30 and 60 meV, it can be observed that there is polaron transport, although the maximum reach of the quasi-particle is still very small. For J_0^y = 20 meV is noted that not only the scope of the polaron is higher than that in the lower degrees of anisotropy but also polaron movement is slowed by this small degree of isotropy. For J_0^y between 0 and 10 meV, on the other hand, the transport is barely retarded because of the high degree of anisotropy. In order to obtain the critical value that defines the different regimes between which the carrier is and is not retarded by the degree of anisotropy, simulations were performed for J_0^y in the interval of [10−20] meV. It was obtained that J_0^y = 17 meV as the maximum value for which the isotropy of the system does not influence the transport. This shows that our model can successfully describe the influence of the anisotropy with respect to the transfer integral, as it has roughly rescued the critical anisotropy level described by previous works in the literature (around 10%).[26] Panel b of the figure also shows how hopping transport occurs in these materials. The oscillation of IPR in time is an expression of the dynamical process. The charge compresses basically into a single molecular unit then expands by distributing itself over two sites and subsequently compressing itself again in the new molecule, finalizing the process of transporting from one molecule to another in the system.

After understanding how the charge transport occurs for different degrees of anisotropy of the transfer integral, we now turn to the discussion of how the system behaves when anisotropy is considered as a function of the e−ph coupling. Because both J_0 and α_2 make up the final value of the transfer integral, the e−ph coupling is directly connected to the lattice deformations. Figure 6 shows the velocity of the charge carrier as a function of α_2^y and J_0^y (both as a ratio to the value in the x-direction). In the figure, it is observed that for the isotropic case of both parameters, the velocity is practically null. On the other hand, it also shows that isotropic transport exists in one of the settings, provided that the other is highly anisotropic. In fact, for J_0^y < 17 meV, there exists the polaron dynamics even if α_2 is isotropic (Figure 5), whereas for $J_0^y = J_0^x$, the velocity begins to increase for α_2^y < 0.24 eV Å^{-1}. Another essential point to be mentioned is that the dynamics is more strongly retarded by the anisotropy of the transfer integral in relation to that of the e−ph coupling. Such anisotropy leads to the highest velocity obtained, including the case when J_0^y = 0 meV and even when compared to α_2^y = 0 eV Å^{-1}. Therefore, a reasonable choice to maintain the two-dimensional characteristics of the polaron and to obtain transport of the charge carrier would be J_0^y and α_2^y equal to 0.6 of the value of the same parameters in the x-direction.

DOI: 10.1021/acs.jpcc.9b00705
J. Phys. Chem. C 2019, 123, 13410−13418

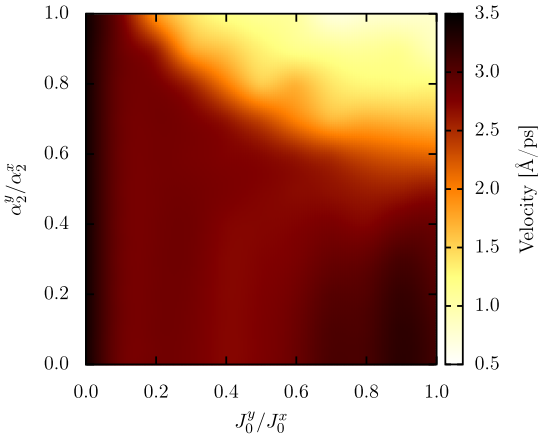

Figure 6. Velocity as a function of J_0^y and α_2^y in relation to the same parameters in the x-direction.

We conclude the present work with an analysis of the behavior of the transport as a function of the electric field. Figure 7 presents the polaron dynamics for a two-dimensional

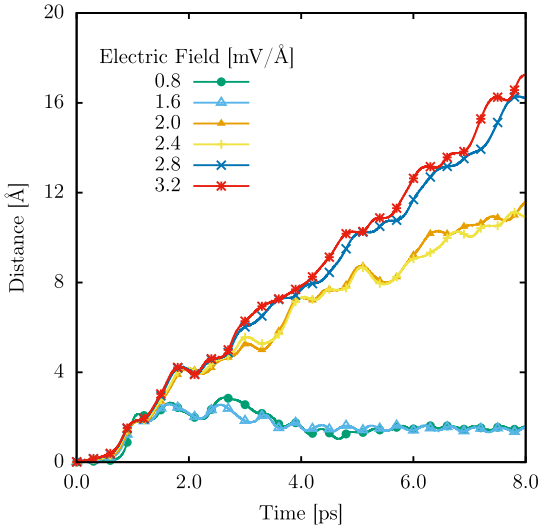

Figure 7. Time evolution of the molecular charge center $x_p(t)$, for a two-dimensional anisotropic system for different external electric fields.

anisotropic hopping with J_0^y = 15 meV and isotropic e−ph coupling. This analysis is carried out so that we can verify the anisotropy effect of hopping and the influence of different electric field intensities over the system irrespective of the direction of propagation. It is possible to observe that for $E_{0x} \leq$ 1.6 mV/Å, the polaron can move very little. For larger electric fields, the range of the polaron is greater, as it would be expected, but its velocities always lie in the subsonic regime. Another essential property to mention is that the polaron does not lose its stability because of the applied electric field strength (3.2 mV/Å is considered relatively high). This shows that the system with one-dimensional characteristics (due to hopping anisotropy) is more stable than the system with distinctly two-dimensional (isotropic) characteristics.

CONCLUSIONS

A Holstein−Peierls model was applied to describe the charge transport in molecular crystals of C_{60}. We investigate the set of parameters used to describe the system, from the static and dynamic properties of the polaron. In our results, we obtain the values of the e−ph couplings that characterize a large polaron solution and verify the anisotropy effects in the stationary configuration of the polaron. Following, we used the obtained geometries to describe the system's dynamics. This was carried out by performing several simulations where the time evolution of the charge carrier was investigated against the effects of anisotropy and the influence of external electric fields. Our results suggest that polaron dynamics occurs in C_{60} when hopping in one direction corresponds to a maximum of 0.17 of the hopping in the other direction. Also, we found that regardless of the degree of anisotropy of the system, the polaron solution appears only in two different ways, with an IPR of approximately 0.5 or 0.75. Concerning different intensities of the electric field, the polaron moves in a subsonic regime and is stable even in the presence of relatively high electric fields (3.2 mV/Å).

ASSOCIATED CONTENT

Supporting Information

The Supporting Information is available free of charge on the ACS Publications website at DOI: 10.1021/acs.jpcc.9b00705.

Schematic representation of the Holstein-Peierls model of the system in a two-dimensional arrangement; set of parameters used in the model Hamiltonian for the triangular lattice; comparison of the stationary polarons properties in square and triangular lattices for a C_{60}-crystal; and comparison of polaron dynamics in square and triangular lattices for a crystal of C_{60} in the presence of external electric field (PDF)

AUTHOR INFORMATION

Corresponding Author

*E-mail: ribeirojr@unb.br.

ORCID

Wiliam Ferreira da Cunha: 0000-0002-4163-9025

Luiz Antonio Ribeiro, Jr.: 0000-0001-7468-2946

Notes

The authors declare no competing financial interest.

ACKNOWLEDGMENTS

The authors gratefully acknowledge the financial support from Brazilian Research Councils CNPq, CAPES, and FAP-DF and CENAPAD-SP for providing the computational facilities. This research work has the support of the Brazilian Ministry of Planning, Development and Management (grants 005/2016 DIPLA—Planning and Management Directorate, and 11/2016 SEST—State-owned Federal Companies Secretariat) and the DPGU—Brazilian Union Public Defender (grant 066/2016). L.A.R.J., W.F.d.C, and G.M.e.S. gratefully acknowledge the financial support from FAP-DF grants 0193.001.511/2017, 0193.001694/2017, and 0193.001766/2017, respectively.

REFERENCES

(1) Shirakawa, H.; McDiarmid, A.; Heeger, A. Twenty-five years of conducting polymers. *Chem. Commun.* **2003**, 1−4.

(2) Epstein, A. J.; Miller, J. S. Linear-chain conductors. *Sci. Am.* **1979**, *241*, 52−61.

(3) Kwon, J. E.; Park, S. Y. Advanced organic optoelectronic materials: Harnessing excited-state intramolecular proton transfer (ESIPT) process. *Adv. Mater.* **2011**, *23*, 3615−3642.

DOI: 10.1021/acs.jpcc.9b00705
J. Phys. Chem. C 2019, 123, 13410−13418

(4) Coropceanu, V.; Cornil, J.; da Silva Filho, D. A.; Olivier, Y.; Silbey, R.; Brédas, J.-L. Charge transport in organic semiconductors. *Chem. Rev.* **2007**, *107*, 926−952.
(5) McCulloch, I.; et al. Semiconducting thienothiophene copolymers: design, synthesis, morphology, and performance in thin-film organic transistors. *Adv. Mater.* **2009**, *21*, 1091−1109.
(6) Li, G.; Zhu, R.; Yang, Y. Polymer solar cells. *Nat. Photonics* **2012**, *6*, 153.
(7) Allard, S.; Forster, M.; Souharce, B.; Thiem, H.; Scherf, U. Organic semiconductors for solution-processable field-effect transistors (OFETs). *Angew. Chem., Int. Ed.* **2008**, *47*, 4070−4098.
(8) Usta, H.; Facchetti, A.; Marks, T. J. n-Channel semiconductor materials design for organic complementary circuits. *Acc. Chem. Res.* **2011**, *44*, 501−510.
(9) Roncali, J.; Leriche, P.; Blanchard, P. Molecular materials for organic photovoltaics: small is beautiful. *Adv. Mater.* **2014**, *26*, 3821−3838.
(10) He, D.; et al. Two-dimensional quasi-freestanding molecular crystals for high-performance organic field-effect transistors. *Nat. Commun.* **2014**, *5*, 5162.
(11) Mozafari, E.; Stafström, S. Polaron dynamics in a two-dimensional Holstein−Peierls system. *J. Chem. Phys.* **2013**, *138*, 184104.
(12) Mozafari, E.; Stafström, S. Polaron stability in molecular crystals. *Phys. Lett. A* **2012**, *376*, 1807−1811.
(13) Song, L.; Shi, Q. A new approach to calculate charge carrier transport mobility in organic molecular crystals from imaginary time path integral simulations. *J. Chem. Phys.* **2015**, *142*, 174103.
(14) Hannewald, K.; Bobbert, P. Ab-Initio Theory of Charge Transport in Organic Crystals. *AIP Conference Proceedings*, 2005; pp 1101−1104.
(15) Wang, L. J.; Li, Q. K.; Shuai, Z. Effects of pressure and temperature on the carrier transports in organic crystal: A first-principles study. *J. Chem. Phys.* **2008**, *128*, 194706.
(16) Tang, L.; Long, M.; Wang, D.; Shuai, Z. The role of acoustic phonon scattering in charge transport in organic semiconductors: a first-principles deformation-potential study. *Sci. China, Ser. B: Chem.* **2009**, *52*, 1646−1652.
(17) Ribeiro, L. A.; Stafström, S. Polaron dynamics in anisotropic Holstein−Peierls systems. *Phys. Chem. Chem. Phys.* **2017**, *19*, 4078−4084.
(18) Ribeiro, L. A.; Stafström, S. Polaron stability in molecular semiconductors: theoretical insight into the impact of the temperature, electric field and the system dimensionality. *Phys. Chem. Chem. Phys.* **2015**, *17*, 8973−8982.
(19) Ribeiro, L. A.; Stafström, S. Impact of the electron−phonon coupling symmetry on the polaron stability and mobility in organic molecular semiconductors. *Phys. Chem. Chem. Phys.* **2016**, *18*, 1386−1391.
(20) Ribeiro, L. A.; Oliveira Neto, P. H.; da Cunha, W. F.; Roncaratti, L. F.; Gargano, R.; da Silva Filho, D. A.; e Silva, G. M. Exciton dissociation and charge carrier recombination processes in organic semiconductors. *J. Chem. Phys.* **2011**, *135*, 224901.
(21) Pandey, R.; Holmes, R. J. Organic Photovoltaic Cells Based on Continuously Graded Donor-Acceptor Heterojunctions. *IEEE J. Sel. Top. Quantum Electron.* **2010**, *16*, 1537−1543.
(22) Li, C.-Z.; Yip, H.-L.; Jen, A. K.-Y. Functional fullerenes for organic photovoltaics. *J. Mater. Chem.* **2012**, *22*, 4161−4177.
(23) Hiraoka, R.; Arafune, R.; Tsukahara, N.; Kawai, M.; Takagi, N. Transport characteristics of a single C 60-molecule junction revealed by multiple Andreev reflections. *Phys. Rev. B: Condens. Matter Mater. Phys.* **2014**, *90*, 241405.
(24) Feng, M.; Zhao, J.; Petek, H. Atomlike, Hollow-Core-Bound Molecular Orbitals of C60. *Science* **2008**, *320*, 359−362.
(25) Reddy, C. D.; Yu, Z. G.; Zhang, Y.-W. Two-dimensional van der waals C 60 molecular crystal. *Sci. Rep.* **2015**, *5*, 12221.
(26) Tamura, H.; Tsukada, M. Role of intermolecular charge delocalization on electron transport in fullerene aggregates. *Phys. Rev. B: Condens. Matter Mater. Phys.* **2012**, *85*, 054301.
(27) Zhou, N.; Huang, Z.; Zhu, J.; Chernyak, V.; Zhao, Y. Polaron dynamics with a multitude of Davydov D2 trial states. *J. Chem. Phys.* **2015**, *143*, 014113.
(28) Wang, L.; Fujihashi, Y.; Chen, L.; Zhao, Y. Finite-temperature time-dependent variation with multiple Davydov states. *J. Chem. Phys.* **2017**, *146*, 124127.
(29) Chen, L.; Zhao, Y.; Tanimura, Y. Dynamics of a One-Dimensional Holstein Polaron with the Hierarchical Equations of Motion Approach. *J. Phys. Chem. Lett.* **2015**, *6*, 3110−3115.
(30) Fujihashi, Y.; Chen, L.; Ishizaki, A.; Wang, J.; Zhao, Y. Effect of high-frequency modes on singlet fission dynamics. *J. Chem. Phys.* **2017**, *146*, 044101.
(31) Huang, Z.; Chen, L.; Zhou, N.; Zhao, Y. Transient dynamics of a one-dimensional Holstein polaron under the influence of an external electric field. *Ann. Phys.* **2017**, *529*, 1600367.
(32) Huang, Z.; Wang, L.; Wu, C.; Chen, L.; Grossmann, F.; Zhao, Y. Polaron dynamics with off-diagonal coupling: beyond the Ehrenfest approximation. *Phys. Chem. Chem. Phys.* **2017**, *19*, 1655−1668.
(33) Wang, L.; Chen, L.; Zhou, N.; Zhao, Y. Variational dynamics of the sub-Ohmic spin-boson model on the basis of multiple Davydov D1 states. *J. Chem. Phys.* **2016**, *144*, 024101.
(34) Zhou, N.; Chen, L.; Huang, Z.; Sun, K.; Tanimura, Y.; Zhao, Y. Fast, Accurate Simulation of Polaron Dynamics and Multidimensional Spectroscopy by Multiple Davydov Trial States. *J. Phys. Chem. A* **2016**, *120*, 1562−1576.
(35) Sun, J.; Luo, B.; Zhao, Y. Dynamics of a one-dimensional Holstein polaron with the Davydov ansätze. *Phys. Rev. B: Condens. Matter Mater. Phys.* **2010**, *82*, 014305.
(36) Luo, B.; Ye, J.; Zhao, Y. Variational study of polaron dynamics with the Davydov Ansätze. *Phys. Status Solidi C* **2011**, *8*, 70−73.
(37) Sun, J.; Duan, L.; Zhao, Y. Delocalized Davydov D1 Ansatz for the Holstein polaron. *J. Chem. Phys.* **2013**, *138*, 174116.
(38) Sun, K.-W.; Gelin, M. F.; Chernyak, V. Y.; Zhao, Y. Davydov ansatz as an efficient tool for the simulation of nonlinear optical response of molecular aggregates. *J. Chem. Phys.* **2015**, *142*, 212448.
(39) Grossmann, F.; Werther, M.; Chen, L.; Zhao, Y. Generalization of the Davydov Ansatz by squeezing. *Chem. Phys.* **2016**, *481*, 99−107.
(40) Pal, A.; Wen, L. K.; Jun, C. Y.; Jeon, I.; Matsuo, Y.; Manzhos, S. Comparative density functional theory-density functional tight binding study of fullerene derivatives: effects due to fullerene size, addends, and crystallinity on band structure, charge transport and optical properties. *Phys. Chem. Chem. Phys.* **2017**, *19*, 28330−28343.
(41) Antropov, V. P.; Gunnarsson, O.; Liechtenstein, A. I. Phonons, electron-phonon, and electron-plasmon coupling inC60compounds. *Phys. Rev. B: Condens. Matter Mater. Phys.* **1993**, *48*, 7651.
(42) Faber, C.; Janssen, J. L.; Côté, M.; Runge, E.; Blase, X. Electron-phonon coupling in the C 60 fullerene within the many-body G W approach. *Phys. Rev. B: Condens. Matter Mater. Phys.* **2011**, *84*, 155104.
(43) Rols, S.; et al. Structure and dynamics of the fullerene polymer Li_4 C_{60} studied with neutron scattering. *Phys. Rev. B: Condens. Matter Mater. Phys.* **2015**, *92*, 014305.
(44) Janssen, J. L.; Côté, M.; Louie, S. G.; Cohen, M. L. Electron-phonon coupling in C_{60} using hybrid functionals. *Phys. Rev. B: Condens. Matter Mater. Phys.* **2010**, *81*, 073106.
(45) Volpi, R.; Kottravel, S.; Nørby, M. S.; Stafström, S.; Linares, M. Effect of Polarization on the Mobility of C60: A Kinetic Monte Carlo Study. *J. Chem. Theory Comput.* **2016**, *12*, 812−824.
(46) Schön, J. H.; Kloc, C.; Batlogg, B. Band-Like Charge Transport in C60 Single Crystals. *Phys. Status Solidi B* **2001**, *225*, 209−213.
(47) Riedmiller, M.; Braun, H. A direct adaptive method for faster backpropagation learning: The RPROP algorithm. Neural Networks. *IEEE International Conference on 1993*, 1993; pp 586−591.
(48) Ono, Y.; Terai, A. Motion of charged soliton in polyacetylene due to electric field. *J. Phys. Soc. Jpn.* **1990**, *59*, 2893−2904.
(49) Reddy, C. D.; Gen Yu, Z.; Zhang, Y.-W. Two-dimensional van der Waals C60 molecular crystal. *Sci. Rep.* **2015**, *5*, 12221.

DOI: 10.1021/acs.jpcc.9b00705
J. Phys. Chem. C 2019, 123, 13410−13418

(50) Ribeiro Junior, L. A.; da Cunha, W. F. Nonadiabatic dynamics of injected holes in conjugated polymers. *Phys. Chem. Chem. Phys.* **2017**, *19*, 10000−10008.
(51) de Oliveira Neto, P. H.; Teixeira, J. F.; da Cunha, W. F.; Gargano, R.; e Silva, G. M. Electron-Lattice Coupling in Armchair Graphene Nanoribbons. *J. Phys. Chem. Lett.* **2012**, *3*, 3039−3042.
(52) Holstein, T. Studies of polaron motion: Part I. The molecular-crystal model. *Ann. Phys.* **1959**, *8*, 325−342.
(53) Holstein, T. Studies of polaron motion: Part II. The small polaron. *Ann. Phys.* **1959**, *8*, 343−389.
(54) Fröhlich, H. Electrons in lattice fields. *Adv. Phys.* **1954**, *3*, 325−361.
(55) Brünger, A.; Brooks, C. L.; Karplus, M. Stochastic boundary conditions for molecular dynamics simulations of ST2 water. *Chem. Phys. Lett.* **1984**, *105*, 495−500.
(56) Izaguirre, J. A.; Catarello, D. P.; Wozniak, J. M.; Skeel, R. D. Langevin stabilization of molecular dynamics. *J. Chem. Phys.* **2001**, *114*, 2090−2098.

DOI: 10.1021/acs.jpcc.9b00705
J. Phys. Chem. C 2019, 123, 13410−13418